

# Local elasticity of strained DNA studied by all-atom simulations

Alexey K. Mazur\*

UPR9080 CNRS, Univ Paris Diderot, Sorbonne Paris Cité,  
Institut de Biologie Physico-Chimique,  
13, rue Pierre et Marie Curie, Paris, 75005, France.

Genomic DNA is constantly subjected to various mechanical stresses arising from its biological functions and cell packaging. If the local mechanical properties of DNA change under torsional and tensional stress, the activity of DNA-modifying proteins and transcription factors can be affected and regulated allosterically. To check this possibility, appropriate steady forces and torques were applied in the course of all-atom molecular dynamics simulations of DNA with AT- and GC-alternating sequences. It is found that the stretching rigidity grows with tension as well as twisting. The torsional rigidity is not affected by stretching, but it varies with twisting very strongly, and differently for the two sequences. Surprisingly, for AT-alternating DNA it passes through a minimum with the average twist close to the experimental value in solution. For this fragment, but not for the GC-alternating sequence, the bending rigidity noticeably changes with both twisting and stretching. The results have important biological implications and shed light upon earlier experimental observations.

PACS numbers: 87.14.gk 87.15.H- 87.15.ap 87.15.ak

## Introduction

Internal mechanical stress is ubiquitous in the biologically active state of double helical DNA. In eucaryotic cells, DNA is densely packed in chromosomes and forced to bend, twist and stretch by numerous protein factors involved in genome regulation [1, 2]. In procaryotes, DNA is subjected to a constitutive unwinding torque maintained by special enzymes, which leads to supercoiling, as in a long rope with bending and twisting elasticity [3, 4]. The supercoiling and, more generally, stress-induced DNA forms are key factors in a variety of cellular processes [5]. For instance, the degree of supercoiling in bacteria changes systematically during the cell cycle and in response to environmental conditions, which is accompanied by activation or suppression of certain genes [6]. The promoter sensitivity to supercoiling stems from the recognition of short promoter elements by RNA polymerase [7]. Detailed studies indicate that it probably does not require DNA melting nor transitions to alternative forms [6]. In *E. coli*, relaxation of the superhelical stress simultaneously alters the activity of 306 genes (7% of the genome), with 106 genes activated and others deactivated [8]. The genes concerned are functionally diverse and widely dispersed throughout the chromosome, and the effect is dose-dependent.

The physical mechanisms of such effects are understood only partially. Long DNA is well described by the coarse-grained worm-like chain (WLC) model [9, 10] supplemented with harmonic twisting and stretching elasticity [11–16]. This model nicely explains the stress-modulated probability of looping, wrapping around proteins, and juxtaposition of distant protein binding sites [17]. However, it cannot account for the promoter sen-

sitivity to supercoiling, for instance, because in this and many other cases the gene regulation has a strong local character and is dominated by sequence effects. A long-discussed hypothesis is that the stress may act as an allosteric factor in protein-DNA recognition [18, 19]. The supercoiling arguably changes the local properties of DNA, as there are small proteins with single short binding sites that can distinguish stressed and relaxed DNA forms [20]; however, it is never clear what exactly is recognized. The supercoiling torque is distributed between twisting and writhing so that the untwisting of the double helix is estimated as 1-2% [21], which is below the thermal noise and too small for reliable recognition. Alternatively, the action of the torsional stress may be conveyed through a property other than the structure of the double helix. For instance, the untwisting may change the elastic parameters of DNA [22–24]. The supercoiled DNA is governed by the interplay between the local bending and twisting fluctuations. If the bending flexibility or the torsional stiffness vary, parameters of thermal fluctuations of short DNA stretches involved in recognition could be noticeably affected even at low levels of stress.

The foregoing hypothesis implies that even with small deformations the DNA elasticity is not exactly harmonic. This possibility was earlier considered in relation to specific experiments and also to explain the discrepancies in twisting rigidity of DNA evaluated by different methods [22–25]. Notably, it was suggested that the stretching forces applied in single molecule measurements and the bending involved in DNA cyclization can increase the apparent twisting rigidity of DNA [25]. The DNA double helix tends to overwind with small stretching [26, 27], but it is not clear if bending and/or stretching affect the twisting elasticity. The mechanical coupling between deformations of different types may be very important for regulation. However, the most interesting for biology is not the overall elasticity, but the behavior of short specific sequences within polymer DNA. To the present,

---

\*Electronic address: alexey@ibpc.fr

all experimental studies have probed only the average properties of long DNA, with a few reports on sequence effects [28, 29] and the influence of supercoiling stress [22–24]. For the free relaxed double helix a good convergence of the results of different experiments is obtained for the bending rigidity [29, 30]. The torsional rigidity has been measured by multiple different techniques, but the results remain controversial [25]. Also, a few estimates of the stretching stiffness have been obtained from nanomechanics experiments with single DNA molecules [14, 31, 32].

Although the local sequence-dependent DNA elasticity and possible stress effects are difficult to reveal experimentally, they can be probed by computer simulations. All-atom molecular dynamics (MD) simulations is a powerful instrument particularly suitable for this purpose. Continuous improvement of forcefields [33–35] and simulation techniques [36, 37] have now made possible free MD simulations that reproduce conformational ensembles of DNA in good agreement with experimental data [38, 39]. Calculated statistics of fluctuations in short DNA qualitatively agree with the WLC theory [40, 41], and the values of the elastic parameters can be measured with good accuracy [42, 43]. DNA deformation is a classical subject of molecular mechanics [44]. In several earlier investigations, all-atom MD simulations were used for studying deformed DNA states obtained by external stretching [45–47], twisting [48–50], or bending [51]. The required deformations were produced by either potential restraints or periodical boundary constraints. A promising alternative method [52] applies steady forces and torques to short stretches of DNA. In contrast to the earlier approaches, this method makes it possible to evaluate elastic parameters under different types and magnitudes of external stress corresponding to physiological conditions. This method captures linear elastic responses as well as the twist-stretch coupling effect under small torques corresponding to a physiological degree of supercoiling [52]. With such approaches it has been found that, depending upon the base pair sequence, small twisting torques corresponding to physiological superhelical density can significantly change the torsional stiffness of the DNA double helix [53].

In this article we present the results of the first systematic study of the influence of external mechanical stress upon the local stretching, twisting, and bending elasticity of the double helical DNA. The numerical algorithms described and tested in the recent reports [52, 53] could be drastically accelerated through parallelization, which made such computations more affordable. Two double helical fragments were considered, with AT- and GC-alternating sequences, respectively. We found that the apparent stretching rigidity of DNA strongly depends upon the method used for measuring the molecule length. When it is obtained by summing base-pair steps as in earlier studies [40, 43, 54] the sign of the twist-stretch coupling effect appears opposite to that measured experimentally. In contrast, much better agreement with ex-

perimental data is obtained when the length is measured directly via the end-to-end distance of one helical turn. We argue that only the latter value corresponds to the experimental observable. The change in the stretching rigidity of DNA with external stress is qualitatively similar for the two sequences. It grows with stretching as well as with increased twisting. The torsional rigidity is essentially unaffected by stretching, but it varies with twisting very strongly, and differently for the two sequences. Surprisingly, for the AT-alternating sequence, it passes through a minimum with the average twist close to the experimental value in solution. For this fragment, but not for the GC-alternating sequence, the bending rigidity noticeably changes with both twisting and stretching. The results shed light upon the earlier experimental observations [22–24] and have important implications for the possible mechanisms of allosteric gene regulation [7, 8, 55].

## Methods

### Simulation protocols

Tetradecamer DNA fragments were modeled with AT-alternating and GC-alternating sequences. A dodecamer fragment is necessary for a full helical turn of a random-sequence B-DNA. The length of 14 base pairs (bp) is minimal for modelling of a helical turn within a longer DNA. This choice of the fragment length and sequences is consistent with and dictated by the results of the earlier studies [42, 43]. Steady stress loads were applied as described elsewhere [52]. This method distributes forces over selected groups of atoms and compensates them by reactions applied to other atoms so as to zero the total external force and torque. Because the forces are applied at different points internal stress and deformations are introduced that correspond to overall twisting or stretching. The method was thoroughly verified in Brownian dynamics simulations of calibrated discrete WLC models [52].

The ranges of forces and torques are selected to comprise the values used in single molecule manipulation experiments as well as the corresponding estimates for living cells. It is known that B-DNA becomes unstable *in vitro* with stretching forces beyond 50 pN [31, 56]. The covalent bonds in long DNA are broken already with forces beyond 300 pN [57], and in living cells DNA is often fragmented during replication in so-called fragile sites [58]. A stretching load of a few tens of piconewtons can be exerted by a single molecule of RNA polymerase during transcription [59, 60], and forces in the nN range pull the chromatids during cell division [61]. The range of torques that do not destroy B-DNA in single molecule experiments is from -10 to +35 pNm [62]. The lower limit is close to the estimated torsional stress due to natural negative supercoiling in procaryotes. These data concern the integral stability of long random sequence DNA.

Short stretches of B-DNA can tolerate much stronger torsional strain. For instance, the DNA twisting observed in complexes with some bacteriophage repressors [63] corresponds to torques beyond 100 pNnm.

The classical MD simulations were carried out by running independent trajectories in parallel on different processors for identical conditions. The number of processors varied between 32 and 48. Trajectories with the lowest loads started from the final states of free dynamics. The amplitudes of forces and torques were increased gradually so that simulations with higher values started from the final states obtained under the preceding lower values. The initial 0.5 ns of every sub-trajectory were discarded, which was sufficient for re-equilibration.

The AMBER98 forcefield parameters [33, 64] were used with the rigid TIP3P water model [65]. The electrostatic interactions were treated by the SPME method [37]. To increase the time step, MD simulations were carried out by the internal coordinate method (ICMD) [66, 67], with the internal DNA mobility limited to essential degrees of freedom. The rotation of water molecules and DNA groups including only hydrogen atoms were slowed down by weighting of the corresponding inertia tensors [68, 69]. The double-helical DNA was modeled with all backbone torsions, free bond angles in the sugar rings, and rigid bases and phosphate groups. The effect of these constraints is insignificant, as was previously checked through comparisons with standard Cartesian dynamics [40, 68]. The time step was 0.01 ps and the DNA structures were saved every 5 ps. All trajectories were continued to obtain the sampling corresponding to 164 ns of continuous dynamics, that is  $2^{15}$  points for every value of force (torque).

Additional technical details including preparation of initial states, treatment of rare events, evaluation of statistical errors, and others are described elsewhere [70].

### Evaluation of elastic parameters

The DNA elasticity is conveniently characterized by three persistence lengths (PLs) corresponding to bending, twisting and stretching that we denote here as  $l_b$ ,  $l_t$ , and  $l_s$ , respectively. These parameters can be extracted from simulated canonical conformational ensembles by using the WLC theory that provides linear relationships of the following form

$$D_x(L) = \frac{L}{l_x} \quad (1)$$

where  $L$  is the DNA length and  $x$  stands for  $b$ ,  $t$ , or  $s$ . The WLC deviations  $D_x(L)$  are computed from appropriate canonical averages as

$$\begin{aligned} D_b(L) &= -\ln(\langle \cos[\theta(L)] \rangle) \\ D_t(L) &= \mathbf{D}[\Phi(L)] \\ D_s(L) &= \left( \frac{2\pi}{3.4 \text{ nm}} \right)^2 \mathbf{D}[L] \end{aligned} \quad (2)$$

where  $\theta(L)$  and  $\Phi(L)$  are the angles of bending and twisting, respectively. The angular brackets denote the canonical averaging and  $\mathbf{D}$  with square brackets refer to the variance of the variable in the brackets. The sampled conformations of the double helix were analyzed by the program 3DNA [71]. Because the elastic parameters should be preferably estimated by using integral numbers of helical turns [43], only 11 central base pair steps (bps) were considered (central dodecamers referred to as TA<sub>6</sub> and CG<sub>6</sub>, respectively). In the following text, symbols  $\theta$ ,  $\Phi$ , and  $L$  denote the corresponding parameters of one helical turn.

According to the standard convention [72], every base pair is characterized by a local Cartesian frame, with the xy-plane parallel to the base pair and z-vectors directed along the DNA. The bend angle  $\theta$  is measured between the z-vectors constructed at the opposite ends of a helical turn. Earlier it was shown that this measure of bending is adequate for integral numbers of helical turns [43]. The torsional fluctuations were probed by three alternative methods. The end-to-end twist,  $\Phi'$ , was evaluated similarly to the local twist [73], but using the two terminal reference frames. The cumulated local twist  $\Phi''$  is obtained by summing the local twist at all base-pair steps. The last angle  $\Phi'''$  is computed similarly by using the base-pair twist with respect to the optimal helical axis. The fluctuations of the DNA length were also evaluated by using three alternative methods. The end-to-end distance,  $L'$  was measured directly between the origins of the terminal reference frames. The contour length  $L''$  was measured by summing the distances between the consecutive frames. The last value,  $L'''$  was obtained by summing the local rise from the 3DNA output. These three methods give different average  $L$  values and it is not evident which of them is the best estimate of the macroscopic DNA length. Therefore, in Eq. (1) we used  $L$  computed as  $11 \cdot 0.335$  nm, that is by using the experimental length for one bps. This can cause a systematic bias in the measured PLs, but does not affect qualitative trends.

## Results

### Two stretching rigidities of the double helix

The length of the double helix is usually evaluated by summing the helical rise along the molecule [40, 54]. The rise can be measured with respect to the helical axis (global rise) or between the base pair frames (local rise). In both cases it is sensitive to algorithmic differences between the analysis programs [74], and the corresponding  $l_s$  values sometimes diverge very significantly [43]. To get reliable estimates we tested several possibilities and three representative techniques outlined in Methods are compared below. The end-to-end distance,  $L'$ , is a direct measure that is adequate in our case because for very short DNA the length fluctuations are dominated

TABLE I Reference zero stress values of the main parameters discussed in the text. The DNA length,  $L$ , the twist,  $\Phi$ , and the corresponding PLs,  $l_s$  and  $l_t$ , respectively, were measured by three alternative methods outlined in Methods. The statistical errors for  $L$  and  $\Phi$  were about 0.4 deg and 0.04 Å, respectively. For  $l_s$  and  $l_t$  the relative errors were about 4% and 5%, respectively.

method	$L$ (Å)		$l_s$ (nm)		method	$\Phi$ (deg)		$l_t$ (nm)	
	TA <sub>6</sub>	CG <sub>6</sub>	TA <sub>6</sub>	CG <sub>6</sub>		TA <sub>6</sub>	CG <sub>6</sub>	TA <sub>6</sub>	CG <sub>6</sub>
$L'$	34.2	35.4	78	172	$\Phi'$	-5.4	15.8	121	123
$L''$	38.7	38.2	230	238	$\Phi''$	349.4	372.6	102	116
$L'''$	36.3	36.4	342	394	$\Phi'''$	365.4	384.0	140	122

by stretching [75, 76]. The second parameter,  $L''$ , is the length of the three-dimensional zigzag line through the origins of the reference frames. By construction,  $L' \leq L''$  (see Table I). The cumulated local rise,  $L'''$ , was used in the earlier studies [43, 54]. The local rise is one of the orthogonal projections of the distance between the neighbor frames, therefore,  $L''' \leq L''$ . A similar value computed with the global rise is not considered here.

Fig. 1 shows the extension-vs-force plots obtained with the above three lengths. All three plots are approximately linear, in good agreement with the harmonic approximation, but the  $L'$  value grows much faster than the other two. Only the vertical positions of the theoretical straight lines were fitted to the data points while the slopes were computed independently, which gives an additional check of self-consistency. The increase of  $L''$  is similar to that of  $L'''$  notwithstanding the divergence of their absolute values (see Table I), and this increase agrees with the  $l_s$  value obtained from equilibrium fluctuations of  $L'''$  rather than  $L''$ . To explain these observations, note that the zigzag probed by  $L''$  forms a helical trace that winds around the straight segment measured by  $L'$ . Fig. 1 suggests that the strokes of the zigzag can be considered inextensible, and the end-to-end distance grows mainly due to flattening of angles. The local helical parameters are obtained by decomposing each stroke of the zigzag into rise, shift and slide [73]. All three of them contribute to the fluctuations of  $L''$ , however, only the rise is affected by the applied force because the other two correspond to displacements nearly orthogonal to the force. This explains why the growth of  $L''$  is better described by  $l_s$  obtained from  $L'''$ .

According to Fig. 1 the double helix is characterized by two qualitatively different stretching rigidities. Parameter  $l'_s$  corresponding to fluctuations of  $L'$  can be measured experimentally. In the experimental literature the stretching stiffness is conventionally characterized by the modulus  $Y_f$  related to  $l_s$  as

$$l_s = \frac{Y_f}{kT} \left( \frac{3.4\text{nm}}{2\pi} \right)^2.$$

The experimental estimates of  $Y_f$  are around 1100 pN [14, 31, 32], which corresponds to  $l_s=78$  nm, in reasonable agreement with  $l'_s$  computed from MD data (see Table I).

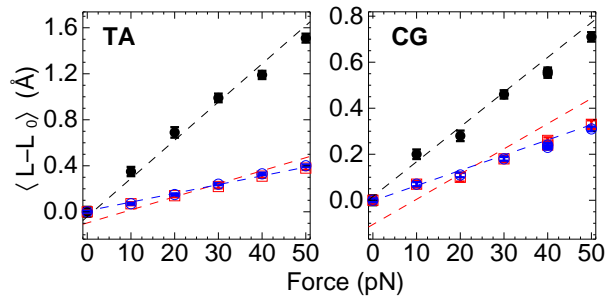


FIG. 1 Color online. DNA extension under steady stretching load. The molecule length was measured by three different methods outlined in the text. The data for  $L'$ ,  $L''$  and  $L'''$  are shown by black dots, open red squares, and open blue circles, respectively. The error bars are small and they merge with symbols. The theoretical harmonic dependences (colored dashed lines) were plotted for the zero-stress values of stretching PL presented in Table I, with the vertical shifts fitted to the data points. The left and right panels exhibit the results for TA<sub>6</sub> and CG<sub>6</sub>, respectively.

This conclusion is corroborated by Fig. 2 that shows how the measured DNA length changes with forced twisting. According to experiments [26, 27] small twisting should cause extension of the double helix. It is seen that the end-to-end length  $L'$  indeed grows with small twisting in quantitative agreement with the experimental estimate.

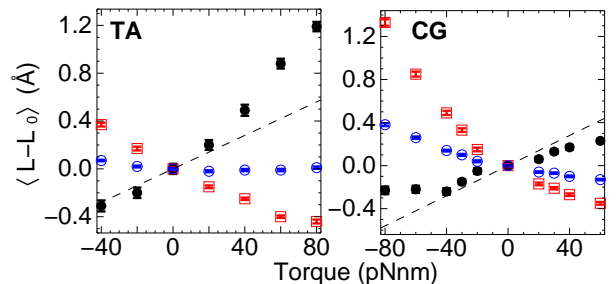


FIG. 2 Color online. Variations of the DNA length under steady twisting torques. The three plots in each panel correspond to alternative definitions of DNA length explained in the text. The notations are same as in Fig. 1. The dotted traces show the expected dependences for a harmonic twist-stretch coupling with parameters measured experimentally [26].

In contrast, the stretching rigidity characterized by parameter  $l'''_s$  is similar for both sequences, but significantly larger than the experimental estimate (see Table I). Thermal fluctuations of the local rise involve perturbations of base-pair stacking, therefore,  $l'''_s$  specifically characterizes the strength of stacking interactions. However, this stretching rigidity is not probed in experiments. Fig. 2 reveals that the lengths measured by parameters  $L''$  and  $L'''$  both decrease with twisting, in qualitative divergence from  $L'$  and experimental observations [26, 27].

The stretching rigidity does not remain constant with forced stretching and twisting. Fig. 3 reveals that in stretched DNA,  $l'_s$  and  $l'''_s$  deviate in opposite senses. The  $l'_s$  value corresponding to experimental measure-

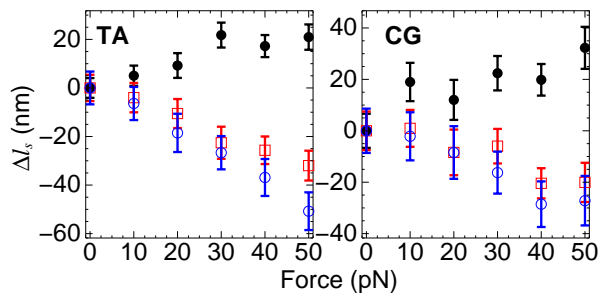


FIG. 3 Color online. Effect of tension upon the stretching rigidity of DNA. The stretching PL was evaluated from the length fluctuations measured by three alternative methods outlined in the text. The reference zero stress values are presented in Table I. The notations correspond to Fig. 1, namely, the data for  $l'_s$ ,  $l''_s$ , and  $l'''_s$  are shown by black dots, open red squares, and open blue circles, respectively.

ments grows. Therefore, the molecule should gradually become stiffer until the stretching force approaches the limit of about 70 pN where the B-DNA is known to loose stability [77]. The stiffening agrees with the deviations of black points in Fig. 1 from the linear plots corresponding to the harmonic approximation. Mechanistically, the growth of  $l'_s$  can be rationalized by noting that, with the zigzag angles flattened, the end-to-end distance  $L'$  approaches the zigzag length  $L''$ . Since  $L'$  can never exceed  $L''$ , the fluctuations of  $L'$  should decrease, that is,  $l'_s$  grows approaching  $l''_s$ . The simultaneous decrease of  $l'''_s$  reflects gradual weakening of base-pair stacking. Twisting also increases the stretching rigidity (see Fig. 4). However, untwisting of TA<sub>6</sub> changes  $l'_s$  only slightly, suggesting that it passes through a minimum with torque  $\tau = -20$  pNm. Interestingly, the value of  $l'_s$  reached with untwisting of CG<sub>6</sub> is similar to that of TA<sub>6</sub>.

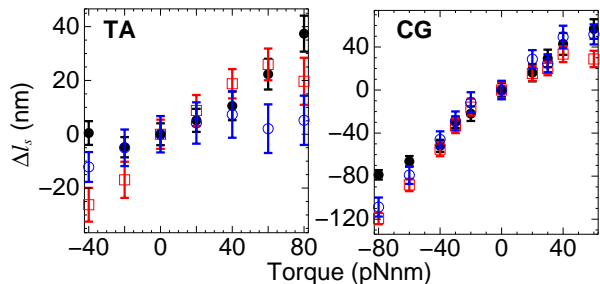


FIG. 4 Color online. Effect of forced twisting upon the stretching rigidity of DNA. The three plots in each panel correspond to alternative definitions of DNA length explained in the text. The notations are same as in 3.

### Torsional rigidity

In the previous report [53] the torsional rigidity was evaluated by using the twist angle  $\Phi'''$  (see Methods). This parameter depends upon the construction of an optimal straight helical axis, which can add a spurious noise

due to bending deformations of the double helix. For verification, here the torsional dynamics are analyzed by three alternative methods including the earlier one. The end-to-end twist  $\Phi'$  is most appropriate for comparisons with experiment because it closely corresponds to that measured in experiments with long DNA. The cumulated local twist  $\Phi''$  represents another reasonable alternative and it was added as an additional check.

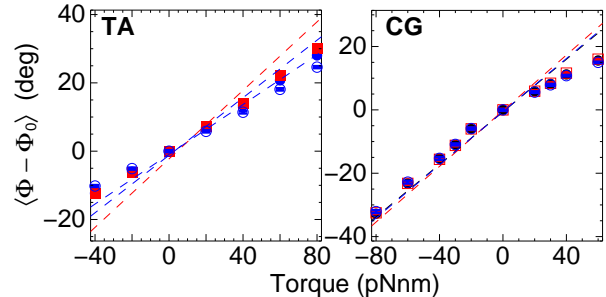


FIG. 5 Color online. DNA twisting under steady torques. The twist angle was measured by three different methods outlined in the text. The data for  $\Phi'$ ,  $\Phi''$ , and  $\Phi'''$  are shown by black dots, open red squares, and open blue circles, respectively. The error bars are small and they merge with symbols. The theoretical harmonic dependences (colored dashed lines) were plotted for the corresponding zero-stress values of the torsional PL presented in Table I, with the vertical shifts fitted to the data points. The left and right panels exhibit the results for TA<sub>6</sub> and CG<sub>6</sub>, respectively.

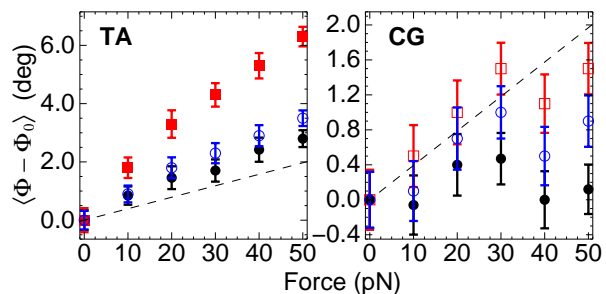


FIG. 6 Color online. Effect of stretching upon DNA twisting. The three plots in each panel correspond to alternative measurements of DNA twisting as explained in the text. The notations are same as in Fig. 5. The dotted traces show the expected dependences for a harmonic twist-stretch coupling with parameters measured experimentally for random-sequence DNA [26].

The external torque changes DNA twisting as shown in Fig. 5. In contrast to stretching, the three alternative measures of angle  $\Phi$  give very similar results in spite of the divergence of the reference zero-stress values (see Table I). Similarly to Fig. 1, only the vertical positions of the theoretical straight lines were fitted to the data points, with the slopes computed independently. This additionally checks the self-consistency and one may note that the deviations from the harmonic law are smaller for  $\Phi'$  and  $\Phi'''$  than for  $\Phi''$ . Earlier single-molecule experiments revealed that DNA overwinds when stretched

[26, 27]. This effect is well reproduced with any of the three methods (see Fig. 6) sometimes with good quantitative agreement. The dashed lines in Fig. 6 represent the experimental dependence for small forces below 30 pN [26]. With stronger extension the twist should start to fall. For TA<sub>6</sub> this experimental observation is not reproduced, but for CG<sub>6</sub> a transition from an ascending trend to an irregular plateau is indeed observed at about 30 pN. This irregular dependence is not due to errors or hidden statistical noise. For verification, we reduced the force from 50 to 40 pN, repeated the MD simulations, then raised the force back to 50 pN, and carried out one more run. The results of this back and forth test were within the error limits shown in Fig. 6.

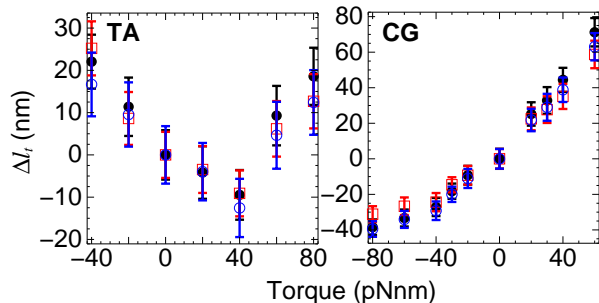


FIG. 7 Color online. Effect of forced twisting upon the torsional rigidity of DNA. The torsional PL was evaluated from the twist fluctuations measured by three alternative methods outlined in the text. The reference zero stress values are presented in Table I. The notations correspond to Fig. 5, namely, the data for  $l_t'$ ,  $l_t''$ , and  $l_t'''$  are shown by black dots, open red squares, and open blue circles, respectively.

The measured torsional rigidity changes with forced twisting as shown in Fig. 7. The three alternative measures of twist yield very similar results all showing strong variations of  $l_t$ , with a remarkable qualitative difference between the two sequences. These rigidity profiles agree with the non-linear features of the  $\Phi(\tau)$  plots in Fig. 5. Indeed, for CG<sub>6</sub> they are concave and for TA<sub>6</sub> the harmonic law corresponding to the zero-stress rigidity overestimates the twisting of both signs. The twisting rigidity of CG<sub>6</sub> grows steadily in the whole range of torques tested. In contrast, for TA<sub>6</sub> an opposite trend is observed under small torques, but  $l_t$  passes via a minimum under positive torques. A qualitatively similar behavior was experimentally observed for one natural DNA sequence [22, 24].

The growth of rigidity with torques of both signs agrees with simple physical intuition for a twist energy profile resembling a flat-bottomed basin with vertical walls. In this case the system cannot go very far even with strong energy fluctuations. The range of torques applied to CG<sub>6</sub> was extended to check the existence of a minimum under negative torques. It is seen, however, that the minimum is not reached although the decrease of  $l_t$  becomes less steep with untwisting. This behavior indicates that anomalously frequent strong untwisting fluctuations

should occur in GC-alternating DNA under normal temperature.

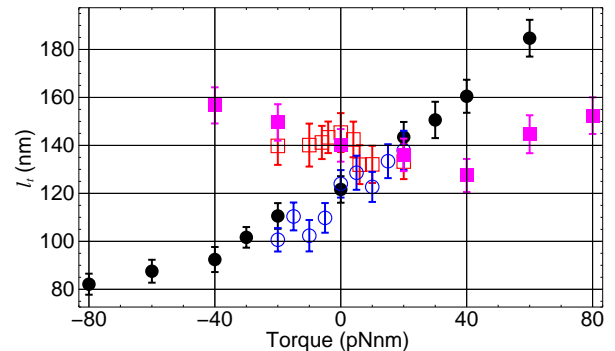


FIG. 8 Color online. Twisting rigidity of DNA under small and large torques. The results of the earlier report [53] (open symbols) are compared with those of the present study (filled symbols). Squares and circles show the data for TA<sub>6</sub> and CG<sub>6</sub>, respectively. The DNA twisting was evaluated by using angle  $\Phi'''$ .

The results in Fig. 7 confirm and corroborate the conclusions of the previous report where smaller torques were considered [53]. The earlier data are compared with those of the present study in Fig. 8. It is seen that the two series of simulations are consistent in spite of the differences in protocols. Each open circle and open square in Fig. 8 correspond to a single continuous trajectory, therefore, this figure confirms ergodicity and validates the much faster protocol introduced here. The new plots also look less noisy, which can be attributed to the absence of slow non-canonical  $\alpha/\gamma$  dynamics. In the previous calculations, such transitions occurred almost exclusively in terminal bps [52, 53], nevertheless, they affected the middle fragments allosterically and contaminated the results.

The strong torsional anharmonicity is not seen in the shapes of the probability distributions of twisting fluctuations of the whole fragment. These distributions remain nearly Gaussian, with the widths changing in agreement with Fig. 7 (see Refs. 53, 70). In contrast, the pattern of single-step twist fluctuations qualitatively explains the effect revealed in Fig. 7 and 8. As seen in Fig. 9, with a notable exception of the adenine-phosphate-thymine steps (ApT), these distributions strongly differ from Gaussians predicted for harmonic WLC model with the measured  $l_t$  values. Surprisingly, for TpA and CpG steps these shapes qualitatively change with twisting. With negative torques the distributions in the upper two panels are strongly positively skewed, but they gradually become negatively skewed as the torque changes the sign. The same is true for the GpC distributions although in this case the effect is much smaller. Some of the TpA and CpG distributions exhibit clear humps suggesting that the twisting in these steps is best described by double-well potentials with low transition barriers.

The CpG and GpC distributions in Fig. 9 behave similarly, that is, they become wider with untwisting in qualitative agreement with the  $l_t(\tau)$  plots for CG<sub>6</sub> in Fig. 8.

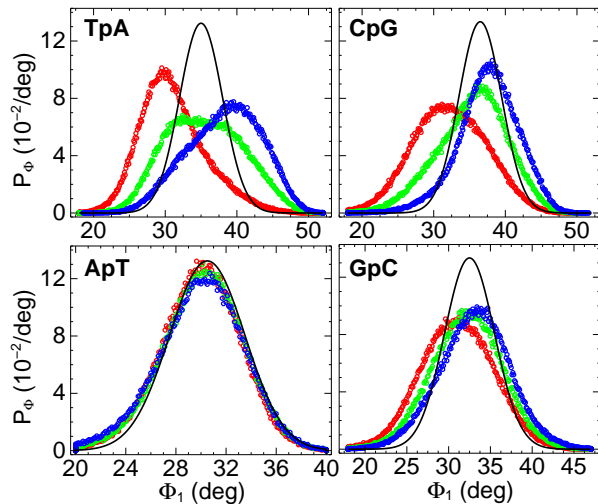


FIG. 9 Color online. The normalized probability densities of twisting fluctuations in the four types of bps represented in  $TA_6$  and  $CG_6$  fragments. Open circles show the computed distributions for strong negative (left, red), medium (middle, green), and strong positive (right, blue) values of external torque, respectively. The corresponding torque values were  $\tau = -40, +40, \text{ and } +80$  pNnm for  $TA_6$  and  $\tau = -40, 0, \text{ and } +40$  pNnm for  $CG_6$ . The black solid lines show the analytical Gaussian distributions for  $l_t$  measured under the middle torque values. These curves are placed to match the maxima of the corresponding computed distributions.

In contrast, in  $TA_6$  the two alternating dinucleotide steps behave differently. The width of the ApT step distributions changes monotonously in the whole range of torques probed, that is, the minimum of  $l_t$  at 40 pNnm in Fig. 8 is exclusively due to TpA steps. The ApT distributions also exhibit a striking feature. The centers of all plots are shifted in agreement with the sign of the applied torque, however, the magnitude of the shift is small compared to the change in the distribution width. As a result, the probabilities of strong untwisting fluctuations are higher with  $\tau = +80$  pNnm than with  $\tau = -40$  pNnm. The effect is small, but statistically significant (see also Ref. 70). This feature is counterintuitive because it cannot be reproduced with the WLC model.

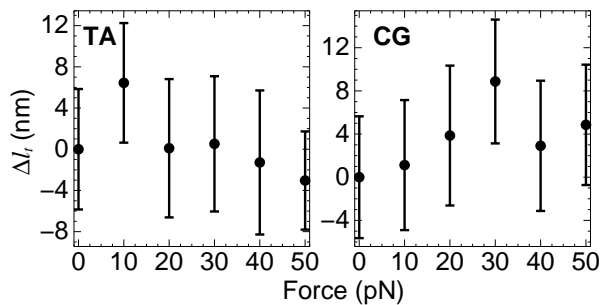


FIG. 10 Effect of stretching forces upon the torsional rigidity of DNA. The measured values of  $l_t$  are shown for  $TA_6$  and  $CG_6$  on the left and right panels, respectively.

In contrast to twisting, small stretching has virtually

no effect upon the torsional rigidity of DNA. The corresponding data are shown in Fig. 10. For clarity, only the  $l_t$  values are shown. The variations are small and rarely exceed the statistical errors. When  $l_t$  is measured by using magnetic tweezers the common stretching load is smaller than 20 pN [62] and the data in Fig. 10 indicate that it can noticeably affect the results only due to mechanisms that are not reproduced in the present DNA model.

## Bending rigidity

In long DNA, stretching naturally flattens bends, whereas twisting causes looping and supercoiling, that is, increases bending in some DNA stretches. These effects are strong; the accompanying changes in the bending rigidity are hardly measurable experimentally and this possibility usually is not considered. The atom-level modeling is the only currently available method that can check whether or not the bending rigidity of DNA in principle can be affected by the twisting and/or tensional stress. The results of the first such tests are shown in Fig. 11.

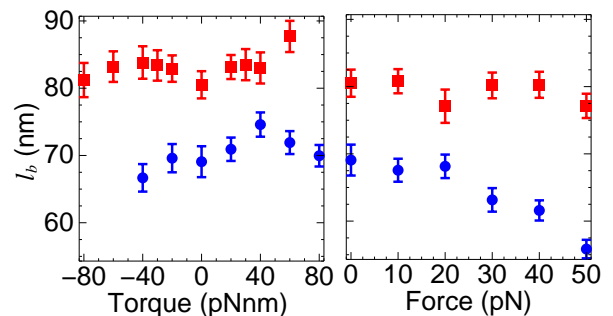


FIG. 11 Color online. Variation of the apparent bending PL with forced stretching and twisting. The results for  $CG_6$  and  $TA_6$  are shown by red squares and blue circles, respectively.

The measured bending PL of  $CG_6$  exhibits only small variations with both twisting and stretching. In contrast, for  $TA_6$  these variations significantly exceed statistical uncertainty and reveal interesting trends. Notably, the right panel of Fig. 11 reveals that bending in  $TA_6$  increases with stretching, which is opposite to the expected flattening effect. At the same time, the  $l_b(\tau)$  dependence in the left panel of Fig. 11 passes through a maximum at 40 pNnm, that is exactly where the torsional PL reaches the local minimum in Fig. 7. A closer look reveals that these trends are accompanied by subtle qualitative changes in the bending dynamics. By using the base pair coordinate frames provided by the program 3DNA [71] one can conveniently characterize the bend direction as follows. Consider two coordinate frames constructed at the first and the last base pairs, respectively. According to the standard convention [72], the two xy-planes dissect the double helix approximately parallel to the base pair

planes. The corresponding two z-vectors approximate the local directions of the helical axis. If the z-vectors are not parallel we can construct the orthogonal projection of the second z-vector upon the first xy-plane. The spherical azimuth angle  $\varphi$  is measured between the projected z-vector and the x-vector of the projection plane. With the x-vector corresponding to the standard convention [72], the value of  $\varphi$  is close to zero when the molecule is bent towards the minor groove in the middle of the helical turn. A few representative distributions of angle  $\varphi$  are shown in Fig. 12.

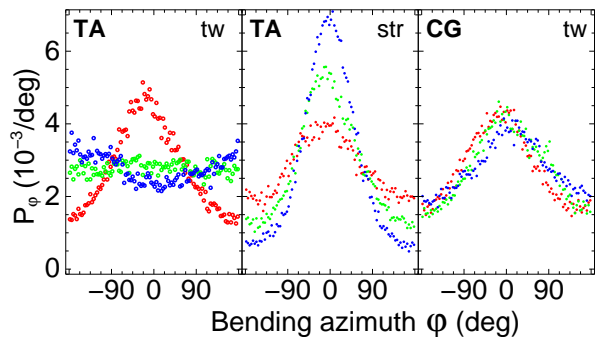


FIG. 12 Color online. Effects of stretching and twisting upon the anisotropy of bending. The normalized probability distributions for the bending azimuth angle  $\varphi$  are shown for TA<sub>6</sub> twisting (left panel) and stretching (middle panel), and for CG<sub>6</sub> twisting (right panel). The red, blue, and green dots correspond to torques  $\tau = -40$ ,  $+40$ , and  $+80$  pNnm (left panel), forces of 0, 20, and 50 pN (middle panel), and torques  $\tau = -80$ , 0, and  $+60$  pNnm (right panel).

The red distribution in the middle panel indicates that the unstressed TA<sub>6</sub> fragment prefers to bend towards the minor groove. The origin of this anisotropy should be studied additionally because it is probably inherent in the overall dynamics rather than caused by local end effects or construction of the coordinate frames. Here we use it just as an indicator. It is seen that the original anisotropy increases with both stretching and unwinding, but positive torques reduce it. As a result, with  $\tau=40$  pNnm the azimuth distribution becomes even, and with further twisting the anisotropy of an opposite sign appears (left panel). This behavior is in remarkable contrast to that of CG<sub>6</sub>. For CG<sub>6</sub> the bending is also preferable towards the minor groove, but twisting only causes rotation of this direction in agreement with the relative orientation of the minor groove in the middle of the fragment (right panel).

Comparison of Fig. 12 with Fig. 7 and 9 suggests that  $\tau=40$  pNnm corresponds to a transition state between two qualitatively different dynamic patterns and that this behavior is attributable to the specific properties of TpA steps. The results in Fig. 7 and 9 can be readily rationalized and qualitatively reproduced in an appropriate coarse-grained model with local twisting described by a double-well potential. Global bending of the double helix results from local deviations of bps geometry described by parameters Roll, Tilt, Slide, and Shift

[72]. Analysis shows that, in TpA steps, all of them are affected by twisting. Roll and Slide change more than other, with Slide exhibiting a bi-modal pattern of fluctuations [70]. These data demonstrate that a mechanical link between twisting and bending is an inherent property of TpA dinucleotides, therefore, we can qualitatively explain the results in the left panel of Fig. 12. The quantitative relation is much more difficult to establish because global bending results from a complex summation of local motions over the whole fragment, including correlations and helical rotation. The correspondence of the transition states for twisting and bending in TA<sub>6</sub> may be a coincidence, nevertheless, the results in Fig. 11 and 12 evidence that twisting and stretching can produce unexpected sequence dependent effects upon the bending dynamics in DNA. The stress response is complex and it cannot be reduced to an altered bending rigidity of the underlying WLC model.

## Discussion

A very good agreement of experiments on polymer DNA with the WLC model [11–16] have led to an exaggerated belief that the harmonic approximation is sufficient for describing all essential properties of the DNA double helix. In fact, these remarkable results cannot be considered as evidences of harmonicity because the additive ladder construction of the double helix effectively hides local heterogeneity and anharmonicity. Due to this additivity, and the central limiting theorem of the probability theory, various experimental data converge to the WLC model regardless of the local DNA properties, with only a few concatenated bps being sufficient for the apparent statistical equivalence with a harmonic elastic rod [53]. This effect shadows the true mechanical properties of the DNA double helix which remain elusive.

The present study evidences that, under normal temperature, the local DNA elasticity is strongly anharmonic, in agreement with the early hypotheses [78] and some experimental data [22–24]. The results of computations using empirical forcefields certainly require further verification. New experimental approaches need to be developed for this purpose because currently available methods can probe only the average elastic parameters of long molecules.

The computed values of all elastic parameters reasonably agree with the data for polymer DNA obtained by different experimental methods. The earlier controversy concerning the stretching (Young’s) modulus [43] is clarified here by comparing different procedures for measuring the length of the double helix. The experimental bending rigidity is characterized by  $l_b \approx 50$  nm [30]. The measured  $l_t$  values vary between 36 and 109 nm depending upon specific methods and conditions [25]. The stretching PL is about 80 nm [14, 31, 32]. MD simulations give somewhat larger values, that is, the DNA stiffness is slightly overestimated. [40, 54] This discrepancy is

not large and it can be attributed to a combination of factors like inexact correspondence between the microscopic geometric parameters and experimental observables, the neutralizing salt conditions in MD, and the small size of the modeled fragments predictably leading to strong sequence and end effects. As shown here, MD also quantitatively reproduce the reciprocal coupling between twisting and stretching revealed in recent magnetic tweezer experiments [26, 27]. The overall agreement is quite remarkable because none of the MD forcefield parameters was adjusted to fit the computed DNA elasticity to experiment. One may reasonably hope, therefore, that the detailed microscopic picture provided by simulations captures the qualitative physical trends dictated by the atom-level mechanics of the double helix.

Our results indicate that the most significant anharmonicity is inherent in the torsional DNA deformations, which is attributable to the special character of stacking interactions. The twisting occurs due to sliding within the stacks; this motion is essentially barrierless and its amplitude significantly exceeds the zone where the harmonic approximation is valid. Even small twisting torques can cause significant changes in elastic parameters. The qualitative difference in the stress response of the torsional rigidity of AT<sub>6</sub> and CG<sub>6</sub> indicates that this property is strongly sequence-dependent. Opposite local trends can mutually cancel out, which makes difficult detection of anharmonic effects in long DNA. There are a few reports in the literature where relevant experimental data qualitatively differ from predictions of harmonic models. This occurred with some natural plasmid DNA [24] and also with synthetic alternating sequences [18]. The latter were recently found anomalous as regards the sequence-dependent bending rigidity [29]. These earlier results require additional investigations.

The mechanical strain is an ubiquitous attribute of living DNA and a key factor in genome packaging and regulation. The common magnitudes of natural forces and torques are quite large, therefore, a wide spectrum of non-linear structural responses should be anticipated, with elastic deformations at one end of the scale, and local melting at the other end. A few anharmonic effects revealed here have some interesting implications for gene regulation mechanisms. According to Fig. 8, with the helical twist slightly shifted from the equilibrium value the sequence dependence of the DNA elasticity can be significantly changed and enhanced. The measured torsional stiffnesses are similar without applied torque, but diverge with both twisting and untwisting. For other sequences, similar behavior can be anticipated for bending and stretching. The deformability of DNA is long considered as a possible governing factor in the sequence-specific site recognition [79], but this mechanism requires strong sequence dependence of local elastic parameters compared to that observed in experiments with long free DNA [28]. As we see the properties of the relaxed DNA cannot be simply transferred to supercoiled and/or protein bound DNA states. Additional studies are necessary

to check if the elastic properties of the specific binding sites are sensitive to external stress.

Unexpectedly, we found that the torsional rigidity of AT<sub>6</sub> passes via a minimum under moderate positive twisting torques. This feature is probably due to a bimodal character of twist fluctuations in the TpA steps (Fig. 9). The average twist of AT<sub>6</sub> with  $\tau=40$  pNnm actually is very close to the experimental value in solution [80, 81] because in free AMBER simulations the DNA structures are somewhat underwound [64]. In this state the TpA steps exhibit a distribution of twist fluctuations corresponding to a saddle point between two domains of attraction (Fig. 9). This point also coincides with the maximum in the measured bending PL accompanied by inversion of the local bending anisotropy.

Earlier it was suggested that the TpA steps can adopt at least two distinct conformational states. Depending on the sequence context, there is always a temperature range where the TpA steps exhibit slow conformational transitions with relaxation times beyond the nanosecond time range [82]. These slow motions should involve extended DNA stretches, that is, these are global transitions accompanied by switching in the TpA steps. The same local switching is probably responsible for the unusual effects observed here. The exceptional properties of the TpA steps are long-known in molecular biology [83]. These steps are found in both narrowings and widenings of the minor B-DNA groove [84, 85]. Periodically spaced TpA steps is the most statistically significant feature of DNA sequences that provide optimal DNA wrapping around nucleosome particles [86]. Switching of local bending anisotropy in response to variable torsional stress may play some role in the control of DNA wrapping and unwrapping. Future studies will show whether or not these processes are related with the unusual microscopic dynamics revealed in our computations.

According to Fig. 9 the strong variation of the twisting rigidity of CG<sub>6</sub> is mainly due to CpG steps. They exhibit anomalously high probability of negative twist fluctuations with torques around zero. The CpG steps are found in a number of known protein binding sites, but their most important biological role is related with C5-cytosine methylation and epigenetic regulation mechanisms [87]. The recognition of CpG sites is a complex multi-facet process because they exist in three methylation states with distinct functions and because specific binding, methylation and demethylation can occur on both free and nucleosome bound DNA [88–91]. Interestingly, methylation of free DNA strongly depends upon supercoiling, with the superhelical density acting smoothly in a dose-dependent manner [92]. The corresponding catalytic mechanism requires cytosine flipping from the DNA stack into a protein pocket [93]. The low energy pathway of this flipping transition may require a strong twisting fluctuation of the CpG step, which would explain the effect of the torsional strain [92].

The above specific examples suggests a more general hypothesis concerning the possible role of strong DNA

fluctuations in gene regulation, with the non-linear elasticity as the governing factor. There are many long-known and well-documented processes *in vivo* where strongly deformed conformations are involved instead of canonical B-DNA. Deformed DNA conformations are ubiquitous in X-ray structures of protein-DNA complexes, so that one may wonder why there is no evolutionary pressure towards proteins that can recognize relaxed B-DNA? It was shown that the activity of promoters regulated via strongly deformed DNA states can be increased by mutations that reduce the deformation energy [55, 94], but these mutations are not selected *in vivo*. It is possible that the prevalence of large DNA deformations is not a trivial consequence of its flexibility, but a necessity of regulatory mechanisms that involve mechanical stress. The larger the deformation - the lower its probability and the population of such state. However, these low probabilities can strongly change in response to small regulatory impulses, in contrast to populations of low energy states. The non-linear elastic effects should play an important role in such regulation because they can greatly amplify the input signal and also make possible complex responses like coupling of the amplitude and the anisotropy of local bending to the torsional stress as in the TA<sub>6</sub> fragment studies here. Similar ideas were discussed in the earlier literature. This hypothesis is complementary to the view of DNA as an allosteric protein cofactor [95] used to explain the smooth modulation of gene activity during cell development [96]. The effects of mechanical strain upon the probabilities of strong fluctuations in DNA represent significant interest and require further studies. New insights in this direction can be obtained by using MD simulations of DNA in steady stress conditions [52] and this work is continued.

### Acknowledgments

The author is grateful to Mickey Schurr and Andrew Travers for useful discussions and valuable comments to the original manuscript.

## I. APPENDIX

### Simulation protocols

Tetradecamer DNA fragments were modeled with AT-alternating (ATATATATATATAT) and GC-alternating (GCCGCGCGCGCGC) sequences. The choice of the fragment length and sequences is consistent with the recent computations [42, 43, 52] and it was dictated by the following considerations. An integral number of helical turns is preferable for evaluation of the elastic parameters of DNA and one helical turn is optimal because of the rapid growth of the principal relaxation times with the chain length [43]. These molecules are homopolymers of ApT and GpC dinucleotides, therefore, they cannot have

distinguished asymmetric structures like static bends. True homopolymer DNA duplexes have special properties and, in free MD with the AMBER forcefield, these structures deviate from the canonical B-DNA stronger than AT- and GC-alternating sequences [97].

The classical MD simulations were carried out by running independent trajectories in parallel on different processors for identical conditions. The number of processors varied between 32 and 48. The starting states were prepared as follows. The solute in the canonical B-DNA conformation [98] was immersed in a 6.2-nm cubic cell with a high water density of 1.04. The box was neutralized by placing Na<sup>+</sup> ions at random water positions at least 5 Å from the solute. The system was energy minimized and dynamics were initiated with the Maxwell distribution of generalized momenta at low temperature. The system was next slowly heated to 293 K and equilibrated during 1.0 ns. After that the water density was adjusted to 0.997 by removing the necessary number of water molecules selected randomly at least 5 Å from DNA and ions, and the simulations were continued with NVT ensemble conditions. Independent starting states for parallel trajectories were prepared by redistributing the counterions around DNA and re-equilibrating the system with different random sets of initial momenta. The statistical independence was verified as explained further below. Steady stress loads were applied as described elsewhere [52]. Trajectories with the lowest loads started from the final states of free dynamics. The amplitudes of forces and torques were increased gradually so that simulations with higher values started from the final states obtained under the preceding lower values. The initial 0.5 ns of every sub-trajectory were discarded, which was sufficient for re-equilibration.

The AMBER98 forcefield parameters [33, 64] were used with the rigid TIP3P water model [65]. The electrostatic interactions were treated by the SPME method [37], with the common values of Ewald parameters, that is 9 Å truncation for the real space sum and  $\beta \approx 0.35$ . The temperature was maintained by the Berendsen algorithm [99] applied separately to solute and solvent with a relaxation time of 10 ps. To increase the time step, MD simulations were carried out by the internal coordinate method (ICMD), [66, 67] with the internal DNA mobility limited to essential degrees of freedom and rotation of water molecules and internal DNA groups including only hydrogen atoms slowed down by weighting of the corresponding inertia tensors. [68, 69] The double-helical DNA was modeled with all backbone torsions, free bond angles in the sugar rings, and rigid bases and phosphate groups. The effect of these constraints is insignificant, as was previously checked through comparisons with standard Cartesian dynamics [40, 68]. The time step was 0.01 ps and the DNA structures were saved every 5 ps. All trajectories were continued to obtain the sampling corresponding to 164 ns of continuous dynamics, that is 2<sup>15</sup> points for every value of force (torque). Statistical convergence and errors were evaluated by the method of

block averages (see further below).

The terminal base pairs open rather frequently during nanosecond time scale MD, which significantly perturbs the flanking DNA structure. Because this dynamics cannot be averaged during the accessible duration of MD trajectories, we blocked it by applying non-perturbing upper distance restraints as explained elsewhere [52]. A similar approach was used to confine the backbone dynamics to the canonical B-DNA zones. Rare non-canonical  $\gamma^{g+} \rightarrow \gamma^t$  switches accompanied by  $\alpha^{g-}/\alpha^{g+}$  and  $\beta^t/\beta^{g+}$  dynamics complicate statistical analysis of MD trajectories [100]. The population of non-canonical conformers is overestimated with all versions of the AMBER94 forcefield including *parmbsc0* [35] most used in recent years [101]. With the *parm98* modifications [64] designed to increase the average DNA twist, this problem seems to be less severe [52]. However, even with a hypothetical ideal forcefield, such transitions should have been blocked because they are too rare for accurate averaging. It appears that the following flat-bottom restraint upon  $\gamma$  torsions solves the problem

$$U_\gamma = \begin{cases} A_\gamma(\gamma - 2\pi/3)^2, & \gamma \geq 2\pi/3 \\ 0, & -\pi < \gamma < 2\pi/3 \end{cases}$$

with  $A_\gamma \approx 30$  kcal/mol. This noninvasive approach does not perturb the dynamics in the canonical zones, which makes possible comparison with the previous long-time simulations of similar DNA fragments.

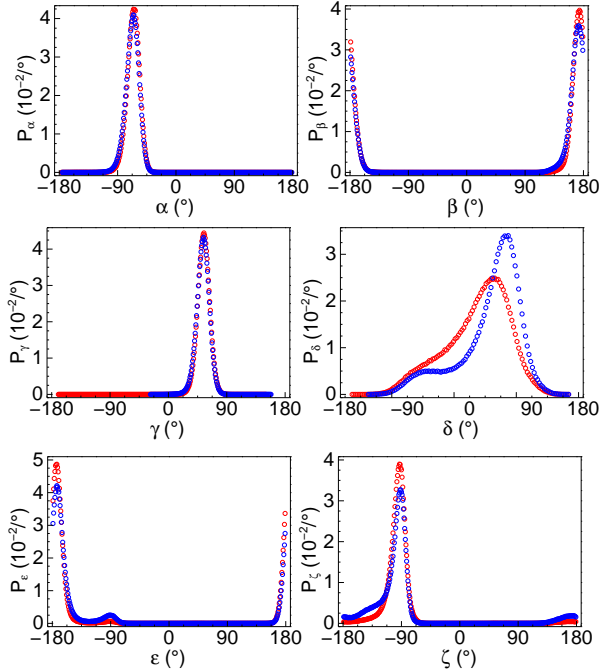


FIG. 1 FIG. 1S: Distributions of backbone torsion angles in free MD simulations of d(ApT)<sub>7</sub> (red circles) and d(GpC)<sub>7</sub> (blue circles).

In all simulations the B-DNA conformations were well conserved without signs of accumulated deformations.

Representative probability distributions of backbone torsions are shown in Fig. 1. They correspond to standard B-DNA dynamics [100].

### Evaluation of statistical errors

Evaluation of errors in MD simulations is based upon the following assertions from the probability theory. Consider a random variable  $x$  with expectation  $\mathbf{M}x = \xi$  and variance  $\mathbf{D}x = \sigma^2$ . We can take  $n$  samples of  $x$  and compute

$$\bar{x} = \frac{1}{n}(x_1 + x_2 + \dots + x_n) = \frac{1}{n} \sum_{k=1}^n x_k$$

and

$$S^2 = \frac{1}{n-1} \sum_{k=1}^n (x_k - \bar{x})^2$$

called the sample average and variance, respectively. Both  $\bar{x}$  and  $S^2$  are random variables, with  $\mathbf{M}\bar{x} = \xi$  and  $\mathbf{M}S^2 = \sigma^2$ , i.e.  $\bar{x}$  and  $S^2$  provide unbiased estimates of  $\xi$  and  $\sigma^2$ , respectively. It is also known that

$$\mathbf{D}\bar{x} = \frac{\sigma^2}{n} \quad (3)$$

and, if  $x$  is a Gaussian random variable,

$$\mathbf{D}S^2 = 2\sigma^4/(n-1). \quad (4)$$

Eq. (3) and (4) are used for evaluation of statistical errors.

Consider evaluation of torsional fluctuations, for instance. In this case, the random variable is the twist angle of one helical turn,  $\Phi$ , with expectation  $\mathbf{M}\Phi$  and variance  $\mathbf{D}\Phi$ . The torsional persistence length is computed as  $l_t = L/\mathbf{D}\Phi$ . The canonical moments  $\mathbf{M}\Phi$  and  $\mathbf{D}\Phi$  are thermodynamic limits and they are estimated by using, respectively, the sample average and variance computed over all  $n$  points saved during an MD trajectory. However, Eq. (3) and (4) cannot be applied straightforwardly because they are valid only for statistically independent samples, i.e. the time intervals between the MD states must be suitably large compared to the torsional relaxation time. The data saving interval is commonly much smaller, therefore, the errors are evaluated by using the method of block averages [102, 103]. The trajectory is successively divided in  $n' = 2, 4, \dots, 2^{15}$  stretches (blocks) and the sample variances  $S'^2$  are computed by using  $n'$  block averages instead of individual samples. When the blocks are longer than the torsional relaxation time the block averages are independent and  $S'^2/n' \approx \text{const} = \sigma^2/\tilde{n}$ , where  $\tilde{n}$  is the effective number of independent samples provided by the trajectory. This value should be used in place of  $n$  in Eq. (3) and (4). In practice, it is convenient to draw the plots of

$$\Omega(n') = \frac{nS'^2}{n'\sigma^2},$$

with respect to  $\log_2 n'$ . When statistical independence is reached, such plots exhibit a plateau with  $\Omega \approx n/\tilde{n} = \tau^c$ , which gives the required estimate of  $\tilde{n}$ . Parameter  $\tau^c$  is the effective correlation time measured in trajectory saving steps.

Fig. 2 shows how this works for Brownian dynamics (BD). We consider eight trajectories from earlier published simulations of a discrete wormlike chain (WLC) model of 14-mer DNA [43, 52]. Each data set involved  $2^{15}$  consecutive configurations saved with a 5 ps interval (about 164 ns in total), that is exactly as in MD simulations. With  $n'$  decreasing, the plots display emergence of a plateau and the growth of statistical noise. The black dashed line displays the results for a single eight times longer trajectory. It is seen that the plateau becomes less noisy, but its level does not change. This confirms the validity of the above derivations, i.e.  $\tau^c$  is constant and, consequently, Eq. (3) holds. Fig. 2 shows that a reasonably accurate estimate of the plateau value can be obtained with  $n' = 2^6$  or larger. On the other hand, the plateau emerges with the block length  $10\tau^c$  or larger, therefore, the lower estimate of the necessary total duration of trajectory is  $640\tau^c$ .

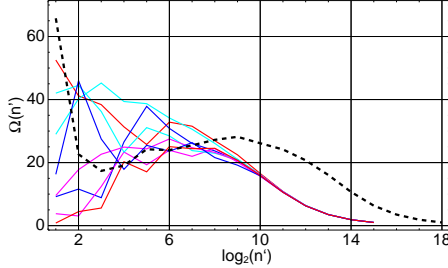


FIG. 2 FIG. 2S: Analysis of statistical errors in BD simulations by the method of block averages [102, 103]. The solid color lines correspond to eight similar 164 ns trajectories. The black dashed line displays the results for a single eight times longer trajectory.

The foregoing analysis is equally valid when several trajectories are concatenated and considered as a single longer trajectory. It is only necessary that the subtrajectories are statistically independent and suitably longer than  $\tau^c$ . A representative example is shown in the upper panel of Fig. 3. We consider the torsional fluctuations of CG<sub>6</sub> fragments. The dashed black plot was obtained by processing a continuous 164 ns trajectory from our earlier report [53]. The solid red line shows the analogous results for the protocol used here (32 concatenated sub-trajectories). In both cases no external stress was applied. The plots show good convergence except for small  $n'$  where the statistical noise is high. The statistical dependence between the subtrajectories is analyzed by using time cross-correlation functions computed as

$$C^{ij}(t) = \frac{\tilde{C}^{ij}(t)}{\tilde{C}^{ij}(0)}; \quad \tilde{C}^{ij}(t) = \langle \Phi^i(\tau + t)\Phi^j(\tau) \rangle_{\tau} - \langle \Phi^i \rangle \langle \Phi^j \rangle \quad (5)$$

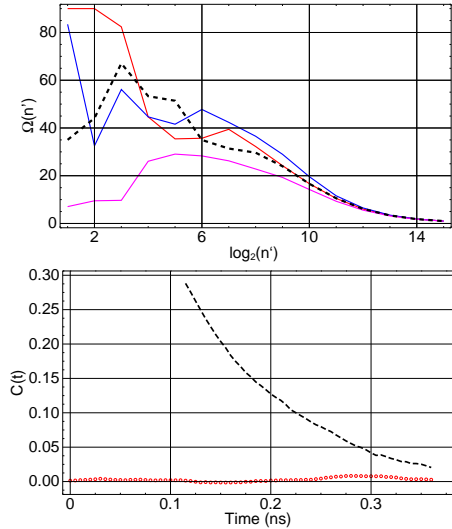


FIG. 3 FIG. 3S: Analysis of statistical errors in MD simulations by the method of block averages [102, 103]. In the upper panel, the solid plots were obtained by concatenating 32 parallel MD trajectories. The red trace shows the results of free dynamics without external stress. Analysis of a continuous 164 ns trajectory with the same total volume of sampling is shown by the black dashed line. The lower panel shows the time autocorrelation function of the  $\Phi$  angle from the continuous trajectory (black dashed trace) and the corresponding average cross-correlation function computed for 32 parallel trajectories (red circles). The blue and magenta traces in the upper panel show the results for applied torques of +40 and -40 pN·nm, respectively.

where the superscripts  $i$  and  $j$  refer to individual subtrajectories. The lower panel compares the cross-correlation function averaged over all  $i \neq j$  with the time autocorrelation function from the long trajectory. The latter is obtained by setting  $i = j$  in Eq. (5). This figure confirms that the subtrajectories are statistically independent from the very beginning. The  $\tau^c \approx 40$  estimated from the upper panel gives  $\tilde{n} = 820$  and the relative error of 4.5% in the measured  $l_t$  values, which is sufficient for our purposes. This relaxation time is approximately two times that estimated from the decay of autocorrelations by using the condition  $C(\tau) = 1/e$ . A similar consistency is observed for BD simulations (see Fig. 2 and Ref. 43).

The upper panel of Fig. 3 displays two additional traces obtained in simulations with applied external torques of  $\pm 40$  pN·nm. The torsional elasticity of the CG<sub>6</sub> fragment changes with the applied torque so that the double helix becomes softer with untwisting. This gives a noticeable increase in the torsional relaxation time, and, accordingly, the three traces corresponding to positive, zero, and negative torques diverge. As a result, for this DNA fragment, the relative error in the measured  $l_t$  values increases with untwisting.

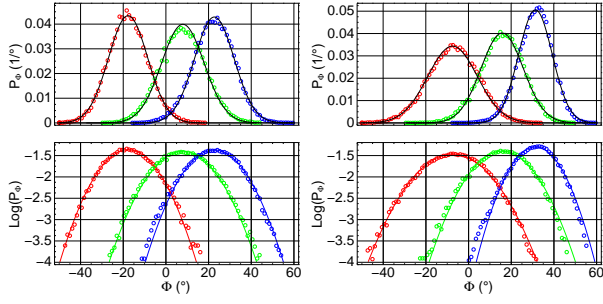


FIG. 4 FIG. 4S: The normalized probability density  $P_\Phi$  under different twisting. Data for TA<sub>6</sub> and CG<sub>6</sub> are exhibited in the left and right columns, respectively. For each fragment, the results are displayed for three representative torque values. For TA<sub>6</sub>, the plots correspond to  $\tau = -40, +40,$  and  $+80$  pN·nm, from left to right, respectively. For CG<sub>6</sub>, the torque values were  $\tau = -40, 0,$  and  $+40$  pN·nm. The analytical distributions Eq. (6) for to the measured values of  $l_t$  and  $\Phi_\tau$  are shown by solid lines. The lower panels display the same data in semi-logarithmic coordinates.

## Results

In a harmonic approximation, the canonical distribution of twisting fluctuations reads

$$P_\Phi \sim \exp \left[ -\frac{l_t}{2L} (\Phi - \Phi_\tau)^2 \right]. \quad (6)$$

where  $\Phi_\tau$  is the shifted equilibrium twist angle under torque  $\tau$ . The persistence length  $l_t$  defines the width of the distribution and it must be constant if the harmonic approximation is valid. The computed patterns of fluctuations appeared qualitatively similar for all three measured twist angles. In Fig. 4, a few representative distributions are exhibited for fluctuations of angle  $\Phi'$ . All of the distributions are close to the analytical Gaussians defined by Eq. (6), however, their widths vary in agreement with the observed changes in  $l_t$ . Systematic deviations from the Gaussian shape are noticeable only with the largest positive torques.

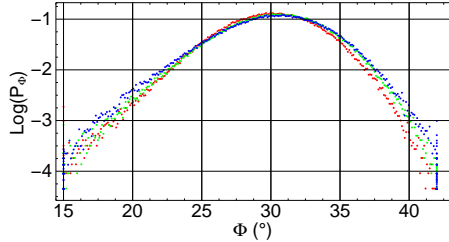


FIG. 5 FIG. 5S: The normalized probability densities of twisting fluctuations in the ApT steps of the TA<sub>6</sub> fragment shown in semi-logarithmic coordinates. The red, green, and blue plots show the data for external torques of  $-40, +40,$  and  $+80$  pN·nm, respectively.

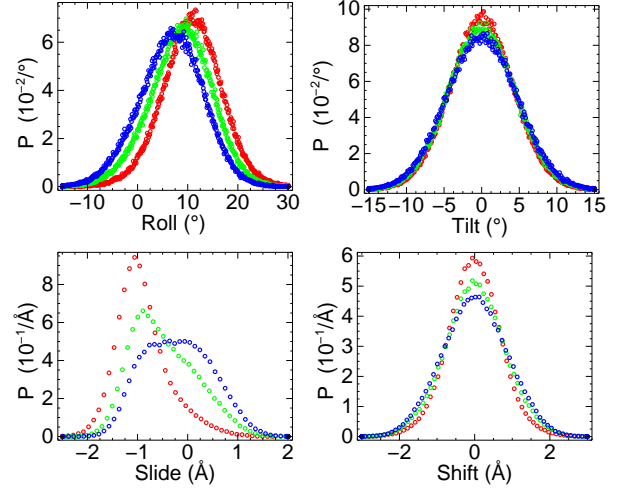


FIG. 6 FIG. 6S: The normalized probability densities of fluctuations of base-step parameters roll, tilt, shift, and slide in TpA dinucleotides of TA<sub>6</sub>. The definition of parameters corresponds to the standard convention. [72] Their values were computed by the program 3DNA. [71] The red, green, and blue plots show the data for torque values  $\tau = -40, +40,$  and  $+80$  pN·nm.

- [1] V. A. Bloomfield, D. M. Crothers, and I. Tinoco, *Nucleic Acids Structures Properties and Functions* (University Science Books, Sausalito, CA, 2000).
- [2] N. R. Cozzarelli, G. J. Cost, M. Nollmann, T. Viard, and J. E. Stray, *Nat. Rev. Mol. Cell. Biol.* **7**, 580 (2006).
- [3] J. C. Wang, *Annu. Rev. Biochem.* **65**, 635 (1996).
- [4] J. C. Wang, *Nature Rev. Mol. Cell Biol.* **3**, 430 (2002).
- [5] A. V. Vologodskii and N. R. Cozzarelli, *Annu. Rev. Biophys. Biomol. Struct.* **23**, 609 (1994).
- [6] A. Travers and G. Muskhelishvili, *Nat. Rev. Microbiol.* **3**, 157 (2005).
- [7] J. A. Borowiec and J. D. Gralla, *J. Mol. Biol.* **195**, 89 (1987).
- [8] B. J. Peter, J. Arsuaga, A. M. Breier, A. B. Khodursky, P. O. Brown, and N. R. Cozzarelli, *Genome Biol.* **5**, R87 (2004).
- [9] L. D. Landau and E. M. Lifshitz, *Statistical Physics, Part 1* (Nauka, Moscow, 1976).
- [10] C. R. Cantor and P. R. Schimmel, *Biophysical Chemistry, Part III: The Behavior of Biological Macromolecules* (W. H. Freeman, San Francisco, 1980).
- [11] C. Bustamante, J. F. Marko, E. D. Siggia, and S. Smith, *Science* **265**, 1599 (1994).
- [12] A. V. Vologodskii, *Macromolecules* **27**, 5623 (1994).
- [13] A. V. Vologodskii and J. F. Marko, *Biophys. J.* **73**, 123 (1997).
- [14] M. D. Wang, H. Yin, R. Landick, J. Gelles, and S. M. Block, *Biophys. J.* **72**, 1335 (1997).
- [15] J. D. Moroz and P. Nelson, *Proc. Natl. Acad. Sci. U. S. A.* **94**, 14418 (1997).
- [16] C. Bouchiat, M. D. Wang, J. Allemand, T. Strick, S. M. Block, and V. Croquette, *Biophys. J.* **76**, 409 (1999).
- [17] A. V. Vologodskii, S. D. Levene, K. V. Klenin, M. Frank-Kamenetskii, and N. R. Cozzarelli, *J. Mol. Biol.* **227**, 1224 (1992).
- [18] R. D. Wells, R. W. Blakesley, S. C. Hardies, G. T. Horn, J. E. Larson, E. Selsing, J. F. Burd, H. W. Chan, J. B. Dodgson, K. F. Jensen, et al., *CRC. Crit. Rev. Biochem.* **4**, 305 (1977).
- [19] W. R. Bauer, *Annu. Rev. Biophys. Bioeng.* **7**, 287 (1978).
- [20] A. Balandina, D. Kamashev, and J. Rouviere-Yaniv, *J. Biol. Chem.* **277**, 27622 (2002).
- [21] T. C. Boles, J. H. White, and N. R. Cozzarelli, *J. Mol. Biol.* **213**, 931 (1990).
- [22] L. Song, B. S. Fujimoto, P. G. Wu, J. C. Thomas, J. H. Shibata, and J. M. Schurr, *J. Mol. Biol.* **214**, 307 (1990).
- [23] P. R. Selvin, D. N. Cook, N. G. Pon, W. R. Bauer, M. P. Klein, and J. E. Hearst, *Science* **255**, 82 (1992).
- [24] A. N. Naimushin, J. B. Clendenning, U. S. Kim, L. Song, B. S. Fujimoto, D. W. Stewart, and J. M. Schurr, *Biophys. Chem.* **52**, 219 (1994).
- [25] B. S. Fujimoto, G. P. Brewwood, and J. M. Schurr, *Biophys. J.* **91**, 4166 (2006).
- [26] J. Gore, Z. Bryant, M. Nollmann, M. U. Le, N. R. Cozzarelli, and C. Bustamante, *Nature* **442**, 836 (2006).
- [27] T. Lionnet, S. Joubaud, R. Lavery, D. Bensimon, and V. Croquette, *Phys. Rev. Lett.* **96**, 178102 (2006).
- [28] B. S. Fujimoto and J. M. Schurr, *Nature* **344**, 175 (1990).
- [29] S. Geggier and A. Vologodskii, *Proc. Natl. Acad. Sci. U. S. A.* **107**, 15421 (2010).
- [30] P. J. Hagerman, *Annu. Rev. Biophys. Biophys. Chem.* **17**, 265 (1988).
- [31] S. B. Smith, Y. Cui, and C. Bustamante, *Science* **271**, 795 (1996).
- [32] J. R. Wenner, M. C. Williams, I. Rouzina, and V. A. Bloomfield, *Biophys. J.* **82**, 3160 (2002).
- [33] W. D. Cornell, P. Cieplak, C. I. Bayly, I. R. Gould, K. M. Merz, D. M. Ferguson, D. C. Spellmeyer, T. Fox, J. W. Caldwell, and P. A. Kollman, *J. Am. Chem. Soc.* **117**, 5179 (1995).
- [34] A. D. MacKerell, Jr., J. Wiórkiewicz-Kuczera, and M. Karplus, *J. Am. Chem. Soc.* **117**, 11946 (1995).
- [35] A. Perez, I. Marchan, D. Svozil, J. Sponer, T. E. Cheatham, C. A. Loughton, and M. Orozco, *Biophys. J.* **92**, 3817 (2007).
- [36] T. Darden, D. York, and L. Pedersen, *J. Chem. Phys.* **98**, 10089 (1993).
- [37] U. Essmann, L. Perera, M. L. Berkowitz, T. Darden, H. Lee, and L. G. Pedersen, *J. Chem. Phys.* **103**, 8577 (1995).
- [38] T. E. Cheatham, III and P. A. Kollman, *Annu. Rev. Phys. Chem.* **51**, 435 (2000).
- [39] A. Perez, F. J. Luque, and M. Orozco, *J. Am. Chem. Soc.* **129**, 14739 (2007).
- [40] A. K. Mazur, *Biophys. J.* **91**, 4507 (2006).
- [41] A. K. Mazur, *Phys. Rev. Lett.* **98**, 218102 (2007).
- [42] A. K. Mazur, *J. Phys. Chem. B* **112**, 4975 (2008).
- [43] A. K. Mazur, *J. Phys. Chem. B* **113**, 2077 (2009).
- [44] V. B. Zhurkin, Y. P. Lysov, and V. I. Ivanov, *Nucleic Acids Res.* **6**, 1081 (1979).
- [45] A. D. MacKerell, Jr. and G. U. Lee, *Eur. Biophys. J.* **28**, 415 (1999).
- [46] S. A. Harris, Z. A. Sands, and C. A. Loughton, *Biophys. J.* **88**, 1684 (2005).
- [47] B. Luan and A. Aksimentiev, *Phys. Rev. Lett.* **101**, 118101 (2008).
- [48] S. Kannan, K. Kohlhoff, and M. Zacharias, *Biophys. J.* **91**, 2956 (2006).
- [49] J. Wereszczynski and I. Andricioaei, *Proc. Natl. Acad. Sci. U. S. A.* **103**, 16200 (2006).
- [50] G. L. Randall, L. Zechiedrich, and B. M. Pettitt, *Nucleic Acids Res.* **37**, 5568 (2009).
- [51] J. Curuksu, K. Zakrzewska, and M. Zacharias, *Nucleic Acids Res.* **36**, 2268 (2008).
- [52] A. K. Mazur, *J. Chem. Theory Comput.* **5**, 2149 (2009).
- [53] A. K. Mazur, *Phys. Rev. Lett.* **105**, 018102 (2010).
- [54] F. Lankas, J. Sponer, P. Hobza, and J. Langowski, *J. Mol. Biol.* **299**, 695 (2000).
- [55] K. L. Chow, M. E. Hogan, and R. J. Schwartz, *Proc. Natl. Acad. Sci. U. S. A.* **88**, 1301 (1991).
- [56] P. Cluzel, A. Lebrun, C. Heller, R. Lavery, J. L. Viovy, D. Chatenay, and F. Caron, *Science* **271**, 792 (1996).
- [57] C. Bustamante, S. B. Smith, J. Liphardt, and D. Smith, *Curr. Opin. Struct. Biol.* **10**, 279 (2000).
- [58] A. Letessier, G. A. Millot, S. Koundrioukoff, A.-M. Lachages, N. Vogt, R. S. Hansen, B. Malfoy, O. Brison, and M. Debatisse, *Nature* **470**, 120 (2011).
- [59] H. Yin, M. D. Wang, K. Svoboda, R. Landick, S. M. Block, and J. Gelles, *Science* **270**, 1653 (1995).
- [60] M. D. Wang, M. J. Schnitzer, H. Yin, R. Landick,

- J. Gelles, and S. M. Block, *Science* **282**, 902 (1998).
- [61] R. B. Nicklas, *J. Cell. Biol.* **97**, 542 (1983).
- [62] Z. Bryant, M. D. Stone, J. Gore, S. B. Smith, N. R. Cozzarelli, and C. Bustamante, *Nature* **424**, 338 (2003).
- [63] G. B. Koudelka, S. A. Mauro, and M. Ciubotaru, *Prog. Nucleic. Acid. Res. Mol. Biol.* **81**, 143 (2006).
- [64] T. E. Cheatham, III, P. Cieplak, and P. A. Kollman, *J. Biomol. Struct. Dyn.* **16**, 845 (1999).
- [65] W. L. Jorgensen, J. Chandreskhar, J. D. Madura, R. W. Impey, and M. L. Klein, *J. Chem. Phys.* **79**, 926 (1983).
- [66] A. K. Mazur, *J. Comput. Chem.* **18**, 1354 (1997).
- [67] A. K. Mazur, *J. Chem. Phys.* **111**, 1407 (1999).
- [68] A. K. Mazur, *J. Am. Chem. Soc.* **120**, 10928 (1998).
- [69] A. K. Mazur, *J. Phys. Chem. B* **102**, 473 (1998).
- [70] See Appendix to this paper.
- [71] X.-J. Lu and W. K. Olson, *Nucleic Acids Res.* **31**, 5108 (2003).
- [72] W. K. Olson, M. Bansal, S. K. Burley, R. E. Dickerson, M. Gerstein, S. C. Harvey, U. Heinemann, X.-J. Lu, S. Neidle, Z. Shakked, et al., *J. Mol. Biol.* **313**, 229 (2001).
- [73] X. J. Lu, M. A. El Hassan, and C. A. Hunter, *J. Mol. Biol.* **273**, 668 (1997).
- [74] X.-J. Lu and W. K. Olson, *J. Mol. Biol.* **285**, 1563 (1999).
- [75] R. S. Mathew-Fenn, R. Das, and P. A. B. Harbury, *Science* **322**, 446 (2008).
- [76] A. K. Mazur, *Phys. Rev. E* **80**, 010901 (2009).
- [77] T. Strick, J. Allemand, V. Croquette, and D. Bensimon, *Prog. Biophys. Mol. Biol.* **74**, 115 (2000).
- [78] J. H. Shibata, J. Wilcoxon, J. M. Schurr, and V. Knauf, *Biochemistry* **23**, 1188 (1984).
- [79] M. E. Hogan and R. H. Austin, *Nature* **329**, 263 (1987).
- [80] D. Rhodes and A. Klug, *Nature* **292**, 378 (1981).
- [81] F. Strauss, C. Gaillard, and A. Prunell, *Eur. J. Biochem* **118**, 215 (1981).
- [82] K. McAteer, P. D. Ellis, and M. A. Kennedy, *Nucleic. Acids. Res.* **23**, 3962 (1995).
- [83] A. A. Travers and A. Klug, *Philos. Trans. R. Soc. Lond. B. Biol. Sci.* **317**, 537 (1987).
- [84] C. Yoon, G. Privé, D. S. Goodsell, and R. E. Dickerson, *Proc. Natl. Acad. Sci. U.S.A.* **85**, 6332 (1988).
- [85] J. R. Quintana, K. Grzeskowiak, K. Yanagi, and R. E. Dickerson, *J. Mol. Biol.* **225**, 379 (1992).
- [86] T. E. Takasuka and A. Stein, *Nucleic. Acids. Res.* **38**, 5672 (2010).
- [87] K. D. Robertson, *Nat. Rev. Genet.* **6**, 597 (2005).
- [88] K. Arita, M. Ariyoshi, H. Tochio, Y. Nakamura, and M. Shirakawa, *Nature* **455**, 818 (2008).
- [89] R. Metivier, R. Gallais, C. Tiffoche, C. L. Peron, R. Z. Jurkowska, R. P. Carmouche, D. Ibberson, P. Barath, F. Demay, G. Reid, et al., *Nature* **452**, 45 (2008).
- [90] K. L. Ho, I. W. McNaie, L. Schmiedeberg, R. J. Klose, A. P. Bird, and M. D. Walkinshaw, *Mol. Cell.* **29**, 525 (2008).
- [91] R. K. Chodavarapu, S. Feng, Y. V. Bernatavichute, P.-Y. Chen, H. Stroud, Y. Yu, J. A. Hetzel, F. Kuo, J. Kim, S. J. Cokus, et al., *Nature* **466**, 388 (2010).
- [92] T. Bestor, *Nucleic. Acids. Res.* **15**, 3835 (1987).
- [93] S. Klimasauskas, S. Kumar, R. J. Roberts, and X. Cheng, *Cell* **76**, 357 (1994).
- [94] X. Li, E. M. Eastman, R. J. Schwartz, and R. Draghia-Akli, *Nat. Biotechnol.* **17**, 241 (1999).
- [95] J. A. Lefstin and K. R. Yamamoto, *Nature* **392**, 885 (1998).
- [96] S. H. Meijnsing, M. A. Pufall, A. Y. So, D. L. Bates, L. Chen, and K. R. Yamamoto, *Science* **324**, 407 (2009).
- [97] A. K. Mazur, *J. Chem. Theory Comput.* **1**, 325 (2005).
- [98] S. Arnott and D. W. L. Hukins, *Biochem. Biophys. Res. Commun.* **47**, 1504 (1972).
- [99] H. J. C. Berendsen, J. P. M. Postma, W. F. van Gunsteren, A. DiNola, and J. R. Haak, *J. Chem. Phys.* **81**, 3684 (1984).
- [100] S. B. Dixit, D. L. Beveridge, D. A. Case, T. E. Cheatham, III, E. Giudice, F. Lankas, R. Lavery, J. H. Maddocks, R. Osman, H. Sklenar, et al., *Biophys. J.* **89**, 3721 (2005).
- [101] F. Lankas, N. Spackova, M. Moakher, P. Enkhbayar, and J. Sponer, *Nucleic. Acids. Res.* **38**, 3414 (2010).
- [102] H. Flyvbjerg and H. G. Petersen, *J. Chem. Phys.* **91**, 461 (1989).
- [103] D. Frenkel and B. Smit, *Understanding Molecular Simulations. From Algorithms to Applications* (Academic Press, New York, 1996).